Improvement of the Electron Momentum Estimation in the CMS Experiment

Jona Hampe

Palaiseau, July 5, 2007

Abstract

An improvement of the electron momentum estimation is presented in the context of the $H \rightarrow ZZ^* \rightarrow e^+e^-e^+e^-$ channel for the Higgs boson decay in the CMS experiment at the LHC collider. First, a correction for the estimation of the electron track momentum and the electron track momentum error is described, followed by the proposition of a new combination of ECAL energy and Tracker momentum.
It is shown that this leads to an improvement of the accuracy of the electron momentum measurement up to 7%. That directly leads to a better reconstruction of the Higgs mass, where the percentage of underestimations is reduced by 8%.

Contents

1 Introduction

The laboratory takes place at the Laboratoire Leprince-Ringuet (LLR) at Ecole Polytechnique, Palaiseau, within the group working on the CMS experiment. An introduction is given starting from the big scale of some 10^4 m of the LHC, moving over to a description of the CMS experiment and a short explanation of the Higgs Boson, ending in section 2 in the small scale of 10^{-19} m of the electron reconstruction.

1.1 CERN and the Large Hadron Collider

The European Organization for Nuclear Research, commonly known as CERN (see figure 1), is the world's largest particle physics laboratory, located just northwest of Geneva on the border between France and Switzerland. The convention establishing CERN was signed on 29 September 1954. From the original 12 signatories of the CERN convention, membership has grown to the present 20 member states. Its main function is to provide the particle accelerators and other infrastructure needed for high-energy physics research. Numerous experiments have been constructed at CERN by international collaborations to make use of them.

Figure 1: The CERN Site and the location of the Large Hadron Collider

The most important and recent project is the Large Hadron Collider (LHC). The LHC is a proton accelerator and collider. Currently nearly finished and after a lot of delays (the most recent one on March 27, 2007 was the incident during a pressure test involving one of the LHC's inner triplet magnet assemblies provided by Fermilab), the LHC is scheduled to begin operation, at reduced energies, in early 2008. It is expected to become the world's largest and highest energy particle accelerator later in 2008, when commissioning at 14 TeV centre of mass energy is completed. The LHC is being funded and built in collaboration with over two thousand physicists from thirty-four countries, universities and laboratories, among which the LLR, Palaiseau and the RWTH, Aachen. When switched on, it is hoped that the collider will produce the elusive Higgs boson particle, the observation of which could explain how elementary particles gain mass and fill in the gap in the Standard Model theory (see section 1.3).

Figure 2: The LHC tunnel

Prior to being injected into the main accelerator, the particles are prepared through a series of systems that successively increase the particle energy levels. The first system is the linear accelerator Linac2 generating 50 MeV protons which feeds the Proton Synchrotron Booster (PSB). Protons are then injected at 1.4 GeV into the Proton Synchrotron (PS) which accelerates them until 26 GeV. The Low-Energy Injector Ring (LEIR) will be used as an ion storage and cooler unit. The Antiproton Decelerator (AD) will produce a beam of anti-protons at 2 GeV, after cooling them down from 3.57 GeV. Finally the Super Proton Synchrotron (SPS) is used to increase the energy of pro-

tons up to 450 GeV, before injecting them into the LHC.
The LHC is contained in a 27 kilometre circumference tunnel located underground at a depth of about 100 metres. The tunnel was formerly used to house the Large Electron-Positron Collider (LEP). The three metre diameter, concrete-lined tunnel actually crosses the border between Switzerland and France at four points, although the majority of its length is inside France (see figure 2).
The collider tunnel contains two pipes enclosed within superconducting magnets cooled by liquid helium, each pipe containing a proton beam. The two beams travel in opposite directions around the ring. The protons will each have an energy of 7 TeV, giving a total collision centre of mass energy of 14 TeV. It will take around ninety microseconds for an individual proton to travel once around the collider. Rather than continuous beams, the protons will be "bunched" together into approximately 2800 bunches, so that interactions between the two beams will take place at discrete intervals never shorter than twenty-five nanoseconds apart. When the collider is first commissioned, it will be operated with fewer bunches, to give a bunch crossing interval of seventy-five nanoseconds.
The size of the LHC constitutes an exceptional engineering challenge with unique safety issues. While running, the total energy stored in the magnets is 10 GJ, and in the beam, 725 MJ. Loss of only 10^{-7} of the beam is sufficient to quench a superconducting magnet. Additional magnets are used to direct the beams to four intersection points where interactions between them will take place. These are the locations of the six experiments using the LHC:

1. ALICE, **A** **L**arge **I**on **C**ollider **E**xperiment
2. ATLAS, **A** **T**oroidal **L**HC **A**pparatu**S**
3. CMS, **C**ompact **M**uon **S**olenoid
4. LHCb, **L**arge **H**adron **C**ollider **b**eauty
5. LHCf, **L**arge **H**adron **C**ollider **f**orward
6. TOTEM, Total Cross Section, Elastic Scattering and Diffraction Dissociation

They are located underground, in large caverns excavated at the LHC's intersection points. Two of them, ATLAS and CMS, are large, "general purpose" particle detectors and direct competitors in finding the Higgs boson. The other four (LHCb, ALICE, TOTEM, and LHCf) are smaller and more specialized. A detailed description of the CMS experiment is given in section 1.2.
The LHC will also be used to collide heavy ions such as lead (Pb) with a collision energy of 1,150 TeV. [1]

1.2 The CMS experiment

As said above, the Compact Muon Solenoid (CMS) experiment is one of two large general-purpose particle physics detectors being built on the proton-proton Large Hadron Collider. Approximately 2300 people from 159 scientific institutes form the CMS experiment. It is located in an underground chamber at Cessy in France, just across the border from Geneva. The overall dimensions of the CMS detector are a length of 21.6 m, a diameter of 14.6 m and a total weight of 12500 tonnes (see figure 3).

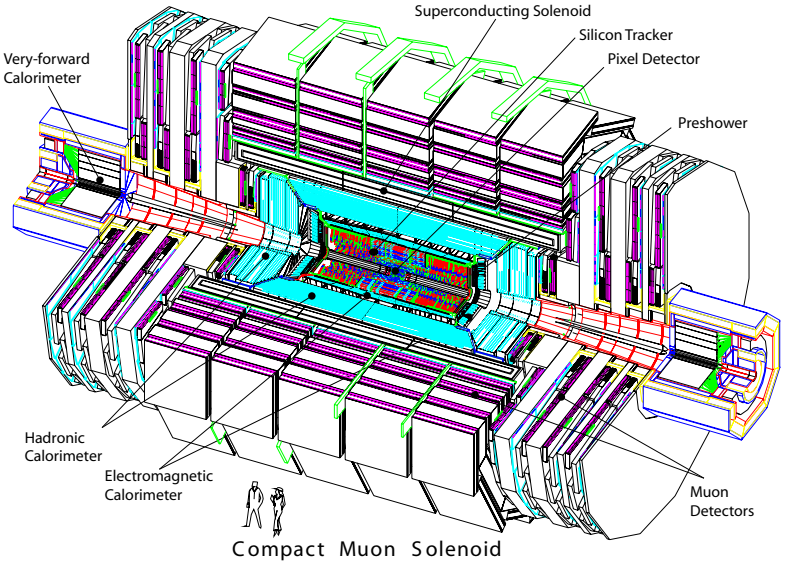

Figure 3: The CMS experiment

1.2.1 Coordinate conventions for the CMS experiment

The coordinate system adopted by CMS has the origin centred at the nominal collision point inside the experiment, the $y-$axis pointing vertically upward, and the $x-$axis pointing radially inward toward the centre of the LHC. Thus, the $z-$axis points along the beam direction toward the Jura mountains from LHC point 5. The azimuthal angle ϕ is measured from the $x-$axis in the $x-y$ plane. The polar angle θ is measured from the $z-$axis. Pseudorapidity is defined as $\eta = -ln(tan\theta/2)$. Thus, the momentum and energy measured transverse to the beam direction, denoted by p_T and E_T, respectively, are computed from the x and y components. [2]

1.2.2 The Experiment

Since CMS (as a part of the LHC) is one of the largest and most expensive experiments in the world operating at a TeV scale the expectations are certainly very high.

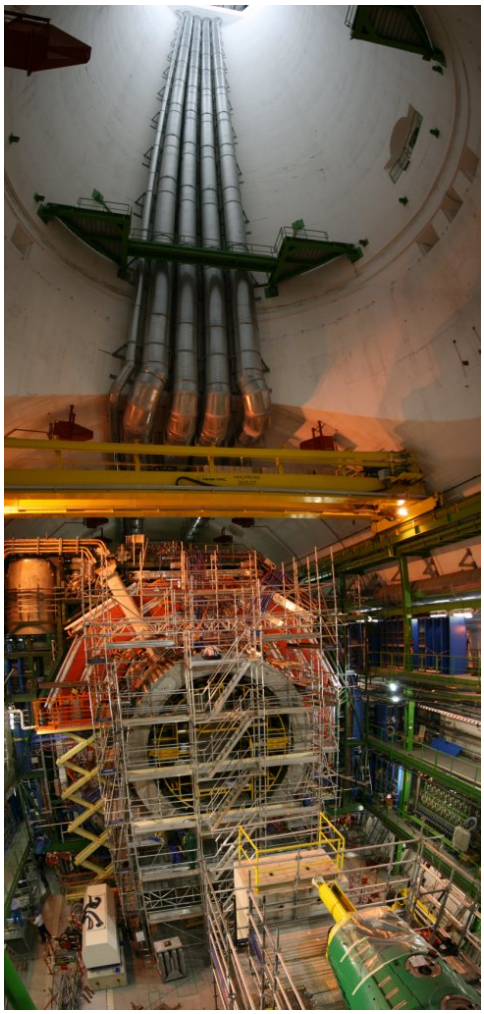

Figure 4: The actual progress of the CMS experiment

The hopes are not "only" to discover the Higgs boson but also to look for evidence of physics beyond the Standard Model, such as super symmetry or extra dimensions and to be able to study aspects of heavy ion collisions. The main distinguishing features of the detector are a high-field solenoid, a full silicon-based inner tracking system, and a fully active scintillating crystals-based electromagnetic calorimeter. The overall layout of CMS is shown in figure 3. At the heart of CMS sits a 13-m-long, 5.9 m inner diameter, 4 T superconducting solenoid. In order to achieve good momentum resolution within a compact spectrometer without making stringent demands on muon-chamber resolution and alignment, a high magnetic field was chosen. The return field is large enough to saturate 1.5 m of iron, allowing 4 muon "stations" to be integrated to ensure robustness and full geometric coverage. Each muon station consists of several layers of aluminium drift tubes (DT) in the barrel region and cathode strip chambers (CDCs) in the endcap region, complemented by resistive plate chambers (RPCs). The bore of the magnetic coil is also large enough to accommodate the inner Tracker and the calorimetry inside. The tracking volume is given by a cylinder of length 5.8 m and diameter 2.6 m. In order ro deal with high track multiplicities, CMS employs 10 layers of silicon microstrip detectors, which provide the required granularity and precision.
In addition, 3 layers of silicon pixel detectors are placed close to the interaction region to improve the measurement of the impact parameter of charged-particle tracks, as well as the position of secondary vertices. [2]

The electromagnetic calorimeter (ECAL) is composed of a barrel covering $|\eta| \leq 1.48$ and two endcaps covering $1.48 < |\eta| \leq 3.0$. The barrel is made of 61200 trapezoidal and quasiprojective crystals. The barrel inner radius is of 124 cm. Viewed from the nominal interaction vertex, the individual crystals appear tilted (off-pointing) by about both 3° in polar and azimuthal angles, and the granularity is about $\Delta\eta \times \Delta\phi = 0.0175 \times 0.0175$ rad. The barrel is divided in two halves, each made of 18 supermodules containing 1700 crystals. Each supermodule is composed of four modules. The endcaps consist of two detectors, a preshower device followed by $PbW0_4$ calorimetry. The preshower is made of silicon strips placed in a 19 cm sandwich of materials including about 2.3 X_0 of Pb absorber. The preshower covers inner radii from 45 cm to 123 cm, corresponding to the range $1.6 < |\eta| \leq 2.6$. Each endcap calorimeter is made of 7324 rectangular and quasi-projective crystals. The crystal front faces are aligned in the (x, y) plane but, as for the barrel, the crystal axes are off-pointing from the nominal vertex in the polar angle by about 3° (see figure 5). [3]

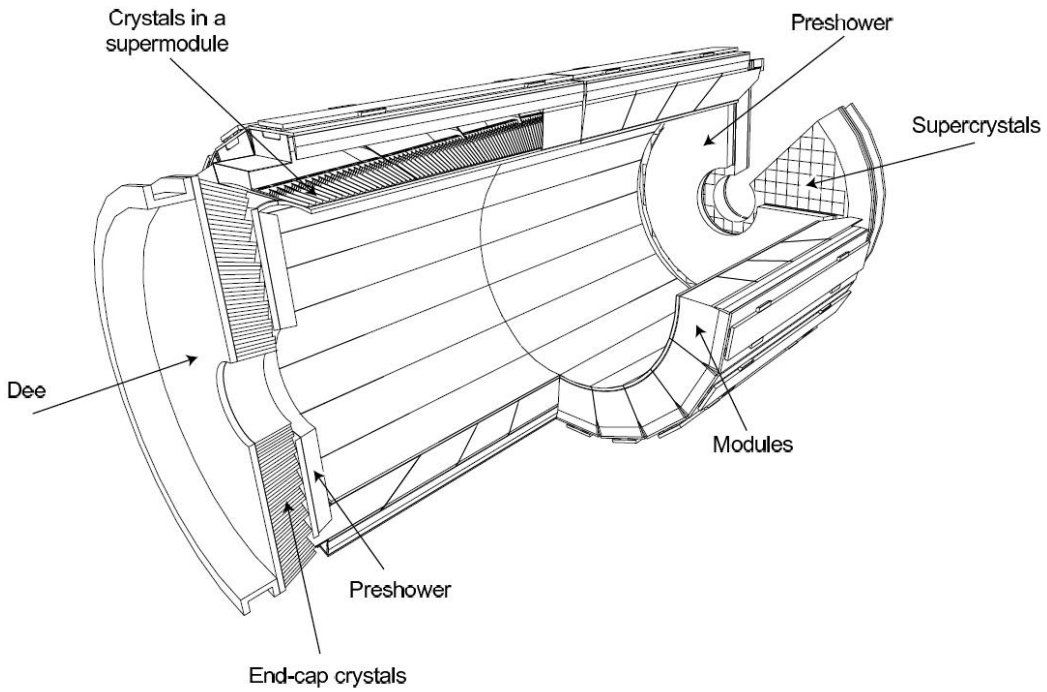

Figure 5: View of the ECAL showing the geometrical arrangement of the modules, the super-modules and the endcaps.

1.3 The Higgs Boson

If the Higgs boson really exists it is - since the discovery of the top Quark at the Fermilab Tevatron in 1995 - one of the last missing pieces of the Standard Model. Following the theory of the Higgs mechanism suggested by Peter Higgs in 1964 [4], a spontaneous break of the electroweak gauge symmetry is responsible for the property of (different) masses of the gauge bosons. Their mass is therefore due to an interaction with a scalar field - called the Higgs field - that permeates the hole universe uniformly. The Higgs boson would be the quantum of this Higgs field. So far the Higgs boson has not been observed in any experiment, despite large efforts invested in accelerator experiments at CERN and Fermilab. The fact that the Higgs boson couldn't be found so far leads to an experimental lower bound for its mass of 114.4 GeV at 95% confidence level. [5]
A more intuitive way of introducing the Higgs mechanism and the Higgs boson is the very famous "quasi-political explanation of the Higgs Boson for Mr Waldegrave, UK Science Minister 1993", in figures 6 and 7. [6]

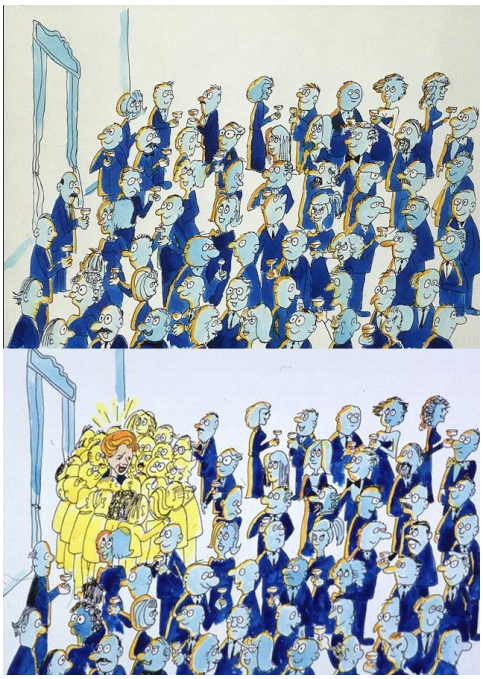

Figure 6: Demonstrative Explanation of the Higgs Field

This explanation begins with the image of a cocktail party of political party workers who are uniformly distributed across the floor, all talking to their nearest neighbours. Then, the ex-Prime-Minister enters and crosses the room. All of the workers in her neighbourhood are strongly attracted to her and cluster round her. As she moves she attracts the people she comes close to, while the ones she has left return to their even spacing. Because of the knot of people always clustered around her she acquires a greater mass than normal, that is, she has more momentum for the same speed of movement across the room. Once moving she is harder to stop, and once stopped she is harder to get moving again because the clustering process has to be restarted. In three dimensions, and with the complications of relativity, this is the Higgs mechanism. In order to give particles mass, a background field is invented which becomes locally distorted whenever a particle moves through it. The distortion - the clustering of the field around the particle - generates the particle's mass.

The second step of the explanation considers a rumour passing through the room full of uniformly spread political workers.

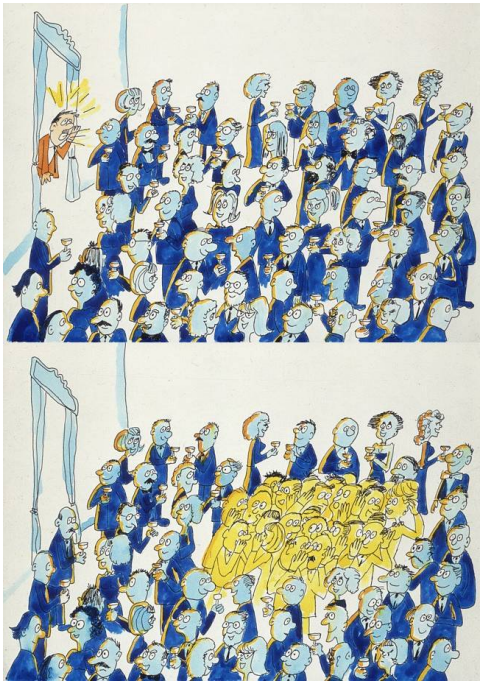

Figure 7: Demonstrative Explanation of the Higgs Particle

Those near the door hear of it first and cluster together to get the details, then they turn and move closer to their next neighbours who want to know about it too. A wave of clustering passes through the room. It may spread out to all the corners, or it may form a compact bunch which carries the news along a line of workers from the door to some dignitary at the other side of the room. Since the information is carried by clusters of people, and since it was clustering which gave extra mass to the ex-Prime Minister, then the rumour-carrying clusters also have mass. The Higgs boson is predicted to be just such a clustering in the Higgs field.

2 Physics context

2.1 The $H \rightarrow ZZ^* \rightarrow e^+e^-e^+e^-$ channel

One of the most promising channels for the search of the Higgs boson at the future LHC pp collider is the single production mode followed by a decay in a ZZ* pair. This inclusive process $pp \rightarrow H + X \rightarrow ZZ^* + X$ is on the critical path of a discovery at the LHC, over an extended range of possible masses of the Higgs boson (m_H).
The value of m_H is a free parameter of the SM which must be constrained by experiments. The range of m_H values at or below the Fermi scale, a scale characteristic of the unification of electromagnetic and weak interactions, is found to be of particular interest.
A consistency fit of electroweak precision data carried out in the SM framework yields an indirect constraint of $m_H < 182\ GeV/c^2$ (at 95% Confidential Level) [7]. Direct searches for the SM Higgs particle at the LEP e^+e^- collider have lead to a strict lower mass bound of 114.4 GeV/c^2 (95% CL). Ongoing direct searches at the Tevatron II p^-p collider by the D0 and CDF experiments could allow to further constrain m_H, to values above $\cong 120\ GeV/c^2$, before the commissioning of the LHC.

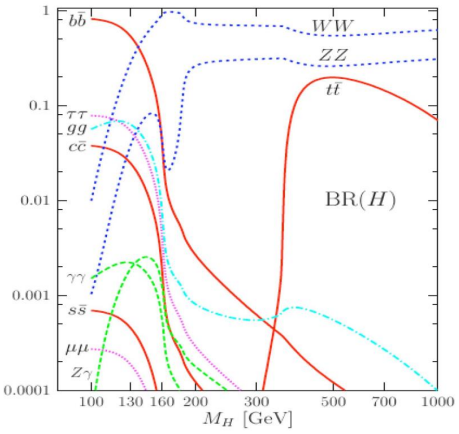

Figure 8: Branching ratios for the Higgs Boson

Figure 8 shows the branching ratios of the Higgs boson as a function of the Higgs mass. The branching ratio in the SM for the $H \rightarrow Z^{(*)}Z^{(*)}$ decay is sizeable ($> 1\%$) for any m_H value above about 115 GeV/c^2. It rises to a peak value above 8% around $m_H > 150\ GeV/c^2$ and is suppressed around $m_H \cong 2m_W$. For $m_H = 2m_Z$, it reaches a plateau of 20 to 30%. The ZZ* contribution, i.e. with at least one Z boson on its mass shell, is greater than 50% for m_H >115 GeV/c^2, and greater than 85% for m_H >150 GeV/c^2. Thus, the $H \rightarrow ZZ^* \rightarrow e^+e^-e^+e^-$ channel offers a possibly significant, very clean and simple multi-lepton final state signature, under the condition of a good electron reconstruction. [8] The aim of this laboratory is to improve the electron momentum evaluation, in order to improve the sensitivity of CMS to the $H \rightarrow ZZ^* \rightarrow e^+e^-e^+e^-$ channel.

2.2 Electron reconstruction and momentum estimation

The reconstruction of the electrons and the estimation of their momentums are done using both, the ECAL and the Tracker detectors.

- In the **ECAL** the electromagnetic showers initiated by electrons (or photons) deposit their energy in several crystals. For a single electron (or photon) reaching the ECAL, most of the energy is collected in a small number of crystals. For a supermodule of the ECAL barrel in the test beam, electrons with an energy of 120 GeV impinging at the centre of a crystal for instance deposit about 97% of their incident energy in a 5×5 crystal window.
  Electrons traversing the Tracker material radiate photons and the energy reaches the ECAL spread in ϕ. Integrated along the electron trajectory the effect can be very large. About 35% of the electrons radiate more than 70% of their initial energy before reaching the ECAL. In about 10% of the cases, more than 95% of the initial energy is radiated. Thus, to obtain a measurement of the electron energy at primary vertex and minimize the cluster containment variations, it is essential to collect bremsstrahlung photons. This is done with the super-clustering algorithms. Starting from the module, where the elctron deposited its energy the algorithms look for modules with separated bremsstrahlung energy next to it and create a supercluster of all those modules.

- The track reconstruction procedure with the **Tracker** in CMS is decomposed into four modular components. Firstly, initial tracks called seeds are looked for with a Seed Generator. Then the Trajectory Builder constructs outward all the possible trajectories for a given seed. With the Trajectory Cleaner ambiguities among the possible trajectories are solved and a maximum number of track candidates is kept. Finally, the final fit of the track is performed with the Trajectory Smoother, which uses all the collected hits to estimate the track parameters at each layer through a backward fit. For electron tracks, in order to better deal with the non-Gaussian fluctuations induced by bremsstrahlung emission, dedicated algorithms have been developed for the seeding and building steps, as well as for the smoothing step where a GSF is used instead of the standard Kalman Filtering (KF) both for forward and the backward fits. [3]

For a more detailed description of the electron reconstruction see [3], [9].

2.2.1 Electron classification

For a further application of the reconstructed electrons it is useful to have information about the quality of the reconstruction. In this paragraph a classification of the reconstructed electrons is given, following [2], [9].

- The **Golden** electron class contains the electrons that are least affected by radiation emission. The reconstructed track matches well with the position of the supercluster and the energy is deposited in a small ϕ range. This class is defined as:
  - a supercluster formed by a single cluster
  - a small bremsstrahlung fraction: $(p_{in} - p_{out})/p_{in} = f_{brem} < 0.2$, where p_{in} is the momentum estimation at the vertex and p_{out} the momentum estimation at the last point of the track measuring
  - ϕ matching between the track extrapolation from last point and the supercluster position within ± 0.15 rad
  - $E/p > 0.9$, where E is the energy given by the ECAL and p the momentum given by the Tracker.
- The **Big Brem** electron class represents all electrons with a high loss of energy due to bremsstrahlung in a single photon but no signs of further energy loss effects from secondary photon conversion. It is defined as:
  - a supercluster formed by a single cluster
  - a bremsstrahlung fraction $f_{brem} > 0.5$
  - $0.9 < E/p < 1.1$
- The **Narrow** electron class is defined as:
  - a supercluster formed by a single cluster
  - $0.9 < E/p < 1.1$
  - a bremsstrahlung fracton or a ϕ not meeting the conditions for Golden or Big Brem electrons
- The **Showering** electron class includes all the electrons that don't fulfil the conditions of the above classes (with an exception of the Crack electrons - see below).
- The **Crack** electron class contains all electrons which have a point of impact near to the space between the modules of the ECAL or between the barrel and the endcap. Their energy can not be measured completely. So far this class only takes the cracks between the supermodules in η and not yet in ϕ into account.

The fraction of the electron classes is strongly correlated with η as can be seen in figure 9.

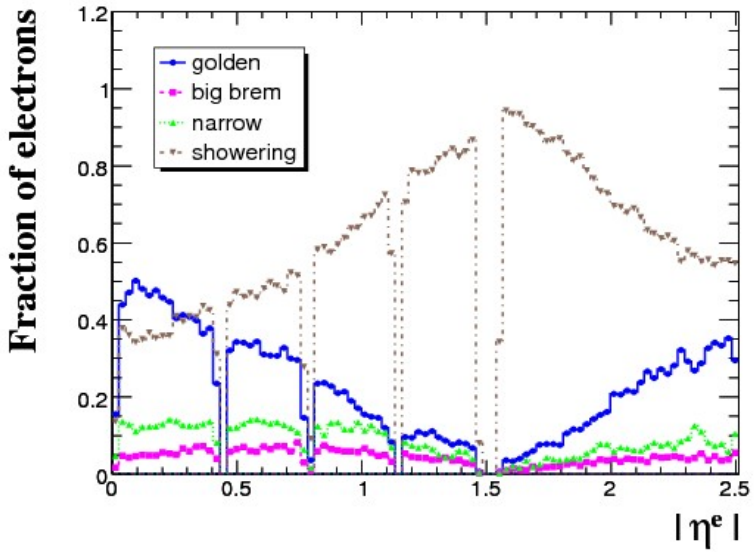

Figure 9: Fraction of electron population in the different classes

2.3 Simulation

In this laboratory the software ROOT for analysis and visualization is used as the programming environment combined with the new CMS software CMSSW.
The way of this work is thereby given by two different approaches. In a first step, the electron track momentum and the electron track momentum error are checked for applicable corrections (see section 3.2, 3.3).
In a second step, the Physics TDR combination (see section 4.1) of the ECAL energy and the Tracker electron momentum is scaned for improvements (see section 4.2).
For these corrections and improvements a 1.5M e^+e^- Monte Carlo sample with energies in between 5 and 100 GeV is used. For the summary of the results and the comparison of the reconstructed Higgs masses, a 63000 $H \rightarrow ZZ^* \rightarrow e^+e^-e^+e^-$ sample is used.

3 Correction of the track momentum and track momentum error

3.1 Approach

To get an insight into the quality of the reconstructed momentum by the Tracker, an analysis of the estimations is performed. The chosen way to study these estimations is to compare electron by electron the reconstructed momentum to the Monte-Carlo generated one, by examining their "Pull"-plots. A "Pull" is hereby considered to be the difference between the estimated (p) and the generated (p_{true}) value of the electron momentum divided by the error given on the estimation (σ_p). If the estimation of the track momentum and its errors is correct, this distribution should be gaussian with a mean equal to zero and a sigma equal to one.

$$Pull = \frac{p - p_{true}}{\sigma_p} \tag{1}$$

This analysis is made for all electrons together (see figure 10) as well as for electrons class per class and seperately for $|\eta| < 1.48$ and $|\eta| \geq 1.48$ (barrel and endcap respectively). In this study an emphasis is put on the gaussian part of the distributions.
The mean of the fitted gaussian is in all cases not equal to zero but slightly shifted. As can be seen in figure 10 the mean of the distribution containing all electron classes in shifted to a value of 0.096 ± 0.002.

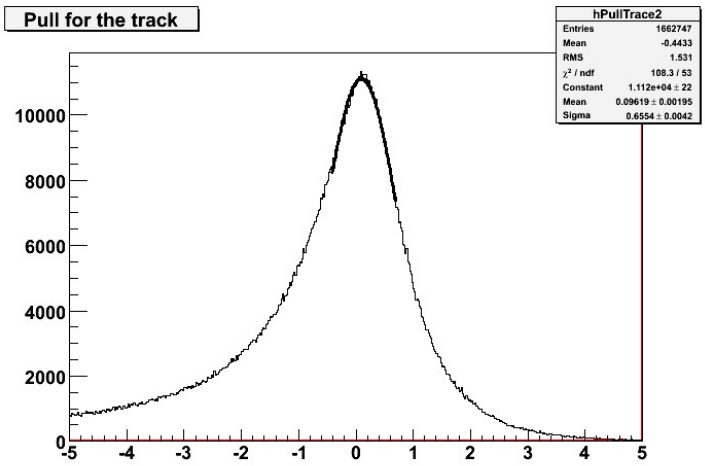

Figure 10: "Pull"-distribution for electrons of all classes

3.2 Correction of the track momentum

The first step is to correct the track momentum. To obtain this correction, (p/p_{true})-distributions are plotted class per class in dependence of p and η in bins of 10 GeV and 0.1 respectively. For each bin, the distribution is fitted by a gaussian and the result of the mean is plotted with its error. As seen in figure 11, a direct correlation between the shift of the mean and p is found but no clear correlation for η can be concluded, as can be seen in figure 12.

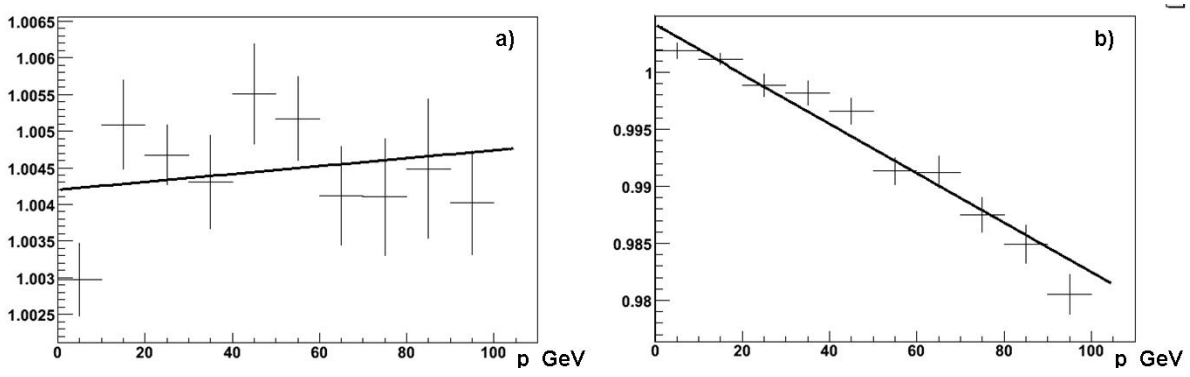

Figure 11: Distribution of the gaussian mean of p/p_{true} as a function of the electron track momentum for a) Golden electrons, b) Showering electrons, in the barrel.

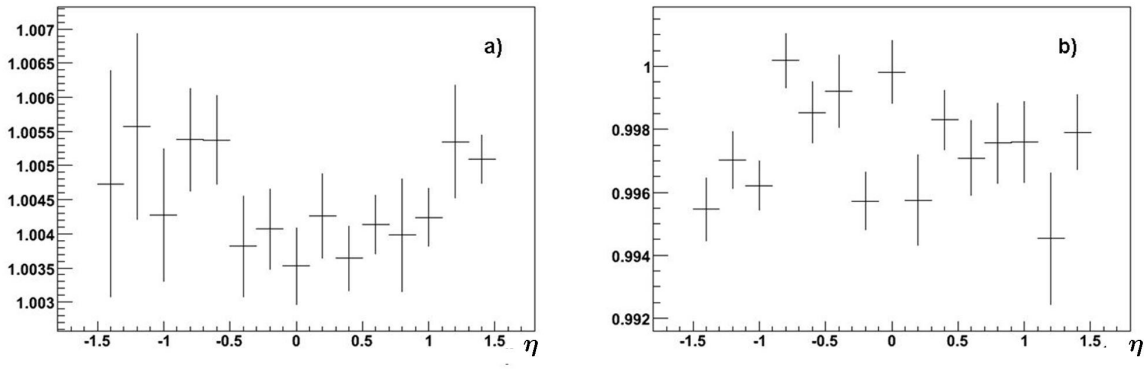

Figure 12: Distribution of the gaussian mean of p/p_{true} as a function of the electron pseudorapidity for a) Golden electrons, b) Showering electrons, in the barrel.

3.2.1 Applied corrections

A linear correlation between the gaussian mean of p/p_{true} and the electron track momentum is found in all treated cases. The applied corrections for the electron momentum as a function of p (f(p)) are given in table 1 for all electron classes. The corrected momentum is therefore given by

$$p_{corr} = \frac{p}{f(p)} \tag{2}$$

No explicit correction is applied as a function of the electron pseudorapidity.

Electron Class	**Correction** $f(p)$
Golden Barrel	$1.004 + 9.66 \cdot 10^{-6} \cdot p$
Golden Endcap	$1.005 + 3.29 \cdot 10^{-5} \cdot p$
Big Brem Barrel	$0.995 + 6.73 \cdot 10^{-5} \cdot p$
Big Brem Endcap	$1.000 + 5.90 \cdot 10^{-5} \cdot p$
Narrow Barrel	$1.006 - 4.65 \cdot 10^{-5} \cdot p$
Narrow Endcap	$1.001 + 2.53 \cdot 10^{-5} \cdot p$
Showering Barrel	$1.004 - 2.16 \cdot 10^{-4} \cdot p$
Showering Endcap	$0.997 - 2.82 \cdot 10^{-4} \cdot p$
Crack	$1.004 - 2.40 \cdot 10^{-5} \cdot p$

Table 1: Applied Corrections for the electron momentum

3.2.2 Results

As can be seen in table 1 corrections of up to about 3 % (for electrons of the Showering class in barrel at 100 GeV) are obtained. For consistency checks, the above described mechanism is applied again after corrections of the electron track momentum. The distributions of the gaussian mean of p/p_{true} as a function of the electron track momentum (figure 13) show that a value of one is obtained with a high precision, proving that the correction is correct.

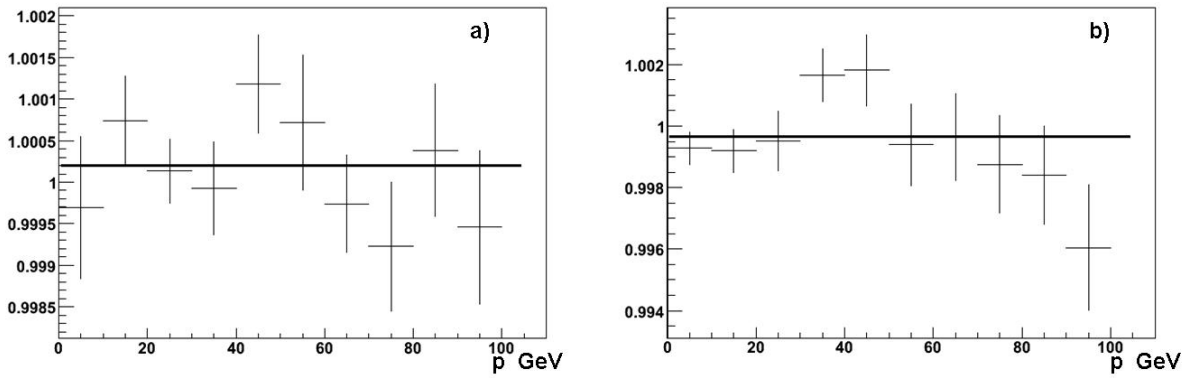

Figure 13: Distribution of the gaussian mean of p/p_{true} as a function of the electron track momentum for a) Golden electrons, b) Showering electrons, in the barrel, after the application of the correction f(p).

Moreover the distributions of the gaussian mean of p/p_{true} as a function of η have now as well an improved value (figure 14), which is a sign of a strong correlation between the estimation of the track momentum and the pseudorapidity.

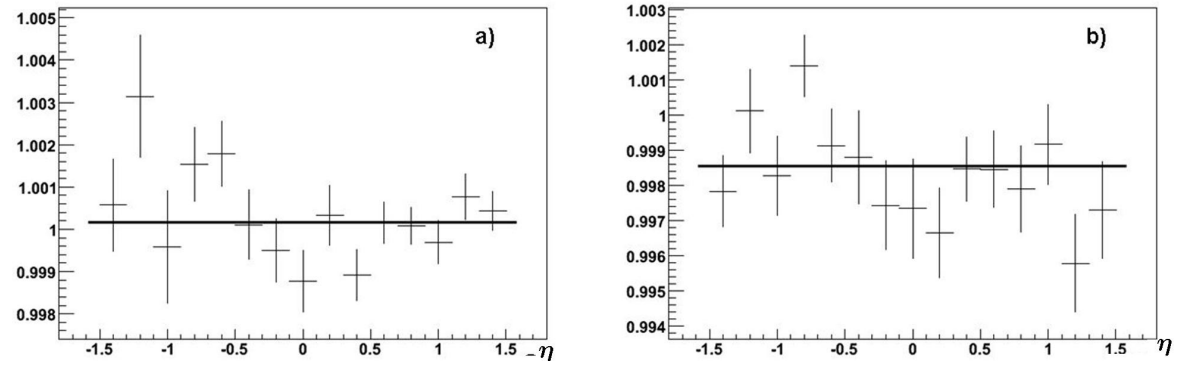

Figure 14: Distribution of the gaussian mean of p/p_{true} as a function of the electron pseudorapidity for a) Golden electrons, b) Showering electrons in the barrel after the application of the correction f(p).

After this correction the shift of the mean of the Pull-distribution is halved for all electrons (see figure 15).

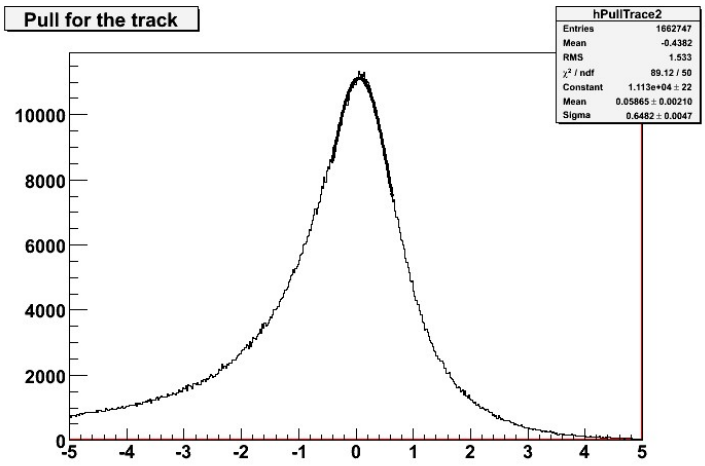

Figure 15: Pull-distribution for electrons of all classes after correction of p

Since the distribution of $(p - p_{true})$ has a mean that is very well centred at zero (see figure 16) the remaining shift is not due to an inaccuracy of the momentum estimation, but is an effect caused by the estimated errors on the electron momentum.

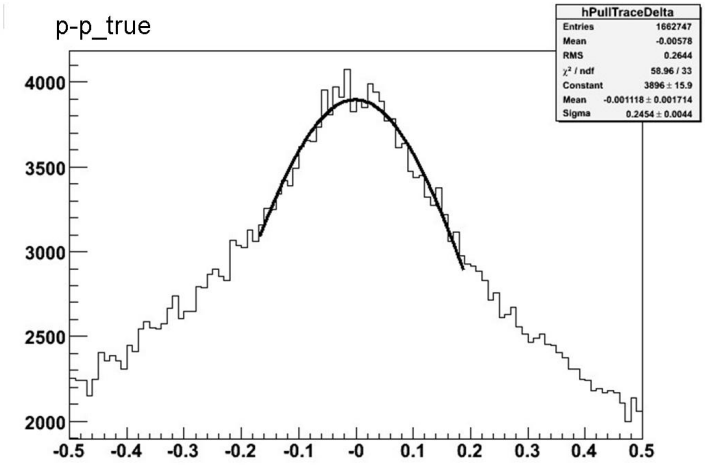

Figure 16: Distribution of $p - p_{true}$ after the application of the correction as a function of the electron momentum

3.3 Correction of the track momentum error

In the second step, the error of the track momentum is corrected. Pull-distributions are plotted class per class in dependence of p and η in bins of 10 GeV and 0.1 respectively. For each bin, the distribution is fitted by a gaussian and the result of sigma is plotted. In contrary to the previous step (see section 3.2) this time no clear general correlation can be found neither as a function of the electron momentum nor as a function of the electron pseudorapidity (see figure 17).

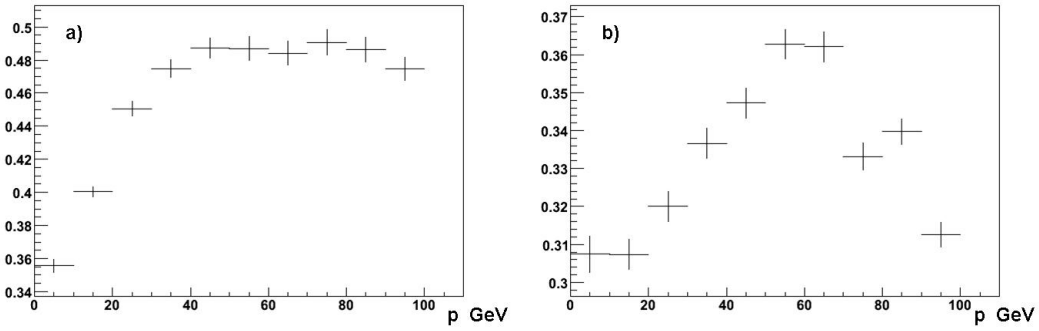

Figure 17: Distribution of the gaussian sigma of the Pull-distributions as a function of the electron momentum for a) Showering electrons, b) Narrow electrons, in the barrel.

Since there is no clear general correlation between gaussian sigma of the Pulls and the electron track momentum or the electron pseudorapidity the first approximation is to find a constant correction for each class of electrons. Here the Pull-distributions are represented class per class, separated into barrel and endcaps (see figures 18, 19 and 20).

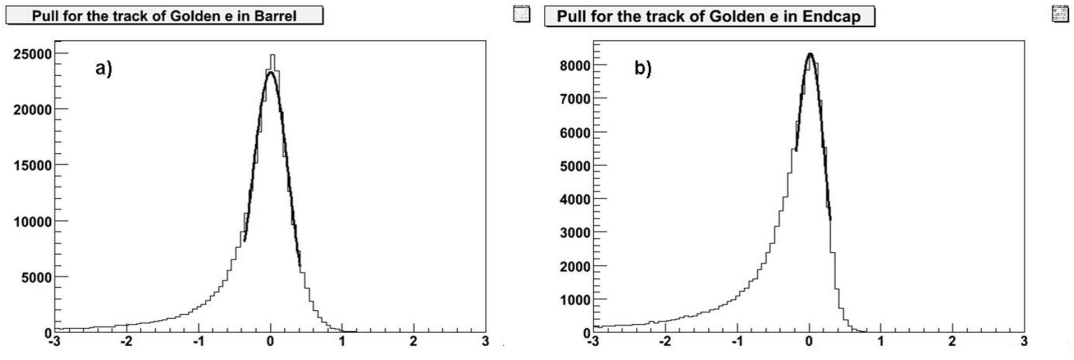

Figure 18: Distribution of the Pull for Golden electrons in the a) barrel, b) endcap

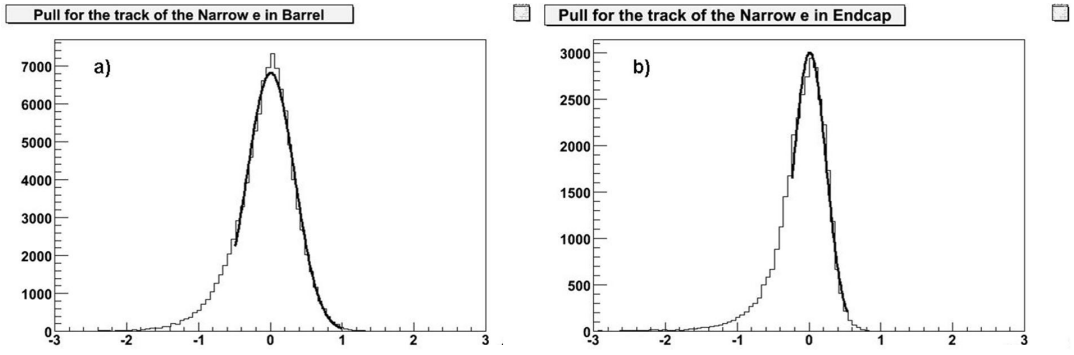

Figure 19: Distribution of the Pull for Narrow electrons in the a) barrel, b) endcap

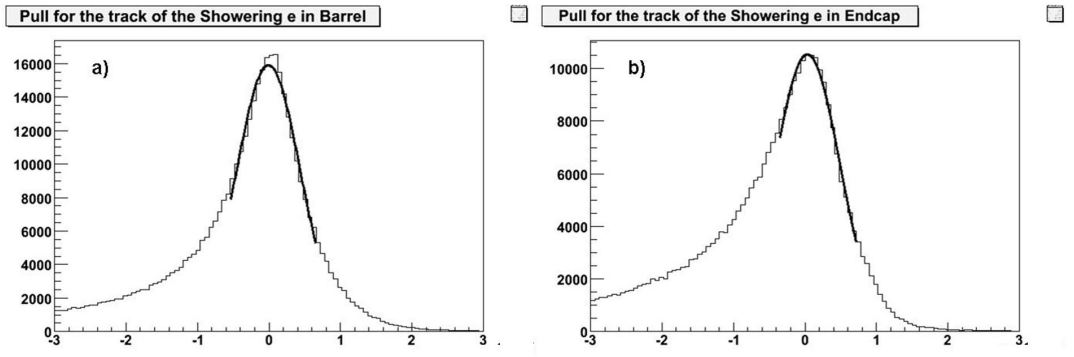

Figure 20: Distribution of the Pull for Showering electrons in the a) barrel, b) endcap

The values for the sigma of the fitted gaussian distributions in figures 18, 19 and 20 can be found in table 2.

3.3.1 Applied corrections

The sigma of the gaussian fitted distributions are considerably below one. This is due to an overestimation of the error on the electron momentum. To improve the estimation of the electron track momentum error, a correction is applied on each electron track momentum error, using the gaussian sigma of the Pull-distributions electron class per electron class. The applied corrections for the error of the electron momentum are given in table 2 for all electron classes. The corrected error is therefore given by

$$\sigma_{p,Corr} = \sigma_p \times c \tag{3}$$

Electron Class	**Correction c**
Golden Barrel	0.214
Golden Endcap	0.206
Big Brem Barrel	0.288
Big Brem Endcap	0.227
Narrow Barrel	0.281
Narrow Endcap	0.234
Showering Barrel	0.384
Showering Endcap	0.439
Crack	0.286

Table 2: Applied Corrections for the error of the electron momentum

It can be concluded that the errors have been overestimated from a factor of about two, for the Showering endcap electrons, up to five, for the Golden endcap electrons (see table 2).

3.3.2 Results

After applying these corrections the sigma of the fitted gaussian of about one can be found for all electron classes separately (see for example figures 21, 22 and 23) as well as for the distribution containing all electrons (see figure 24). The obtained value is $\sigma = 1.023 \pm 0.004$.

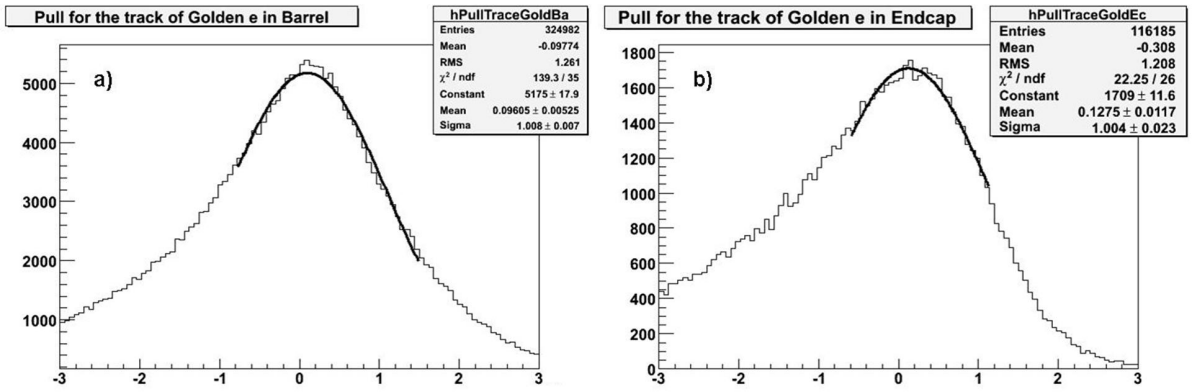

Figure 21: Pull-distribution for electrons of the Golden class after correction of the electron track momentum error for electrons a) in barrel b) in endcaps

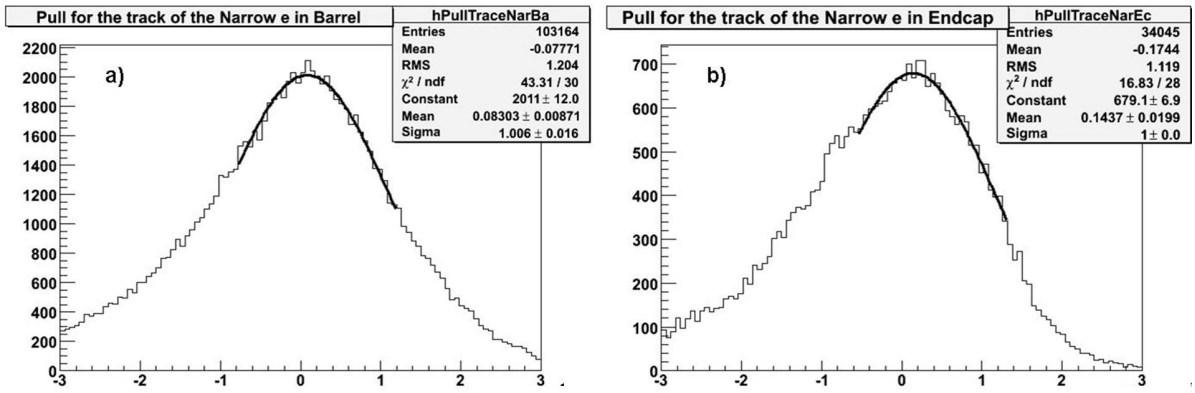

Figure 22: Pull-distribution for electrons of the Narrow class after correction of the electron track momentum error for electrons a) in barrel b) in endcaps

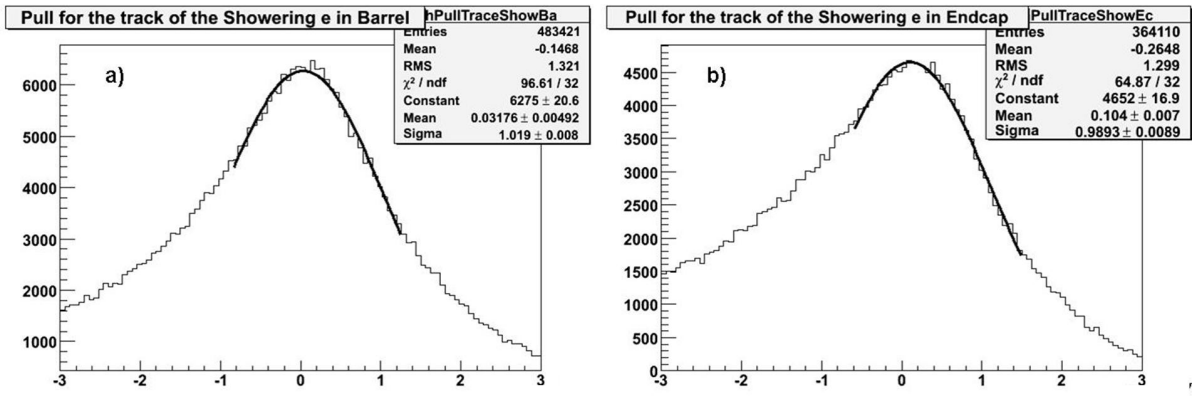

Figure 23: Pull-distribution for electrons of the Showering class after correction of the electron track momentum error for electrons a) in barrel b) in endcaps

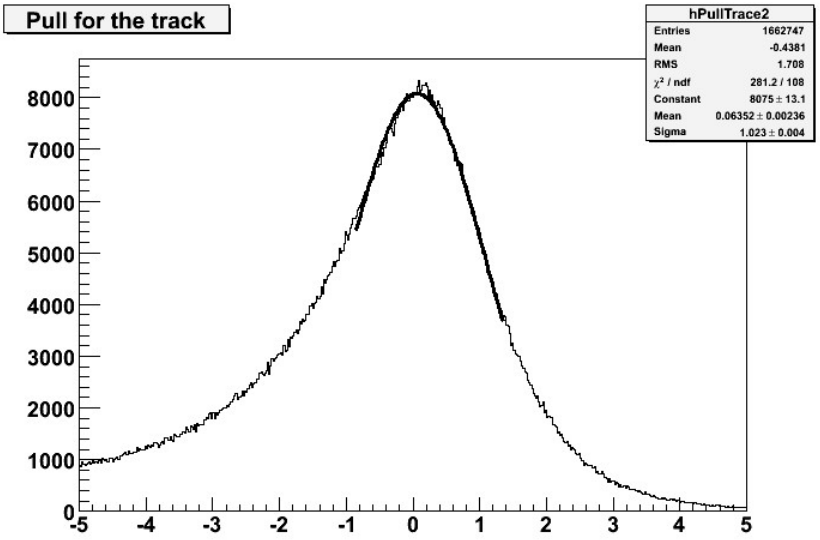

Figure 24: Pull-distribution for electrons of all classes after correction of the electron track momentum error

It can be seen that again the mean of the Pull-distribution is shifted (see figure 24). As seen above (figure 16) the mean of the $p_{corr} - p_{true}$-distribution is well centred at zero. So the shift is a remaining effect caused by the given errors on the electron momentum, even after corrections.

4 Combination of ECAL energy and track momentum

4.1 Physics TDR combination

As explained in section 1 the electron energy is measured by the electromagnetic calorimeter and the electron momentum by the Tracker. The accuracy of the ECAL and the Tracker is not equal, and depends on the energy of the electron. Thus the Tracker momentum estimate is a lot more precise for low energies than the ECAL, whereas for higher energies the estimation of the ECAL is more precise than the Tracker. Moreover, these two measurements are complementary affected by bremsstrahlung radiation in the Tracker material.
To improve the estimation of the electron momentum at the interaction vertex a combination of the energy measurement E of the ECAL and the momentum measured by the Tracker is introduced.
To obtain a combination that takes the best estimation of the ECAL and Tracker into account, it is necessary to study the accuracy of these two instruments. Therefore the ratios E/E_{true} and p_{corr}/p_{true} as a function of E/p were analysed (see figure 25 and 26).

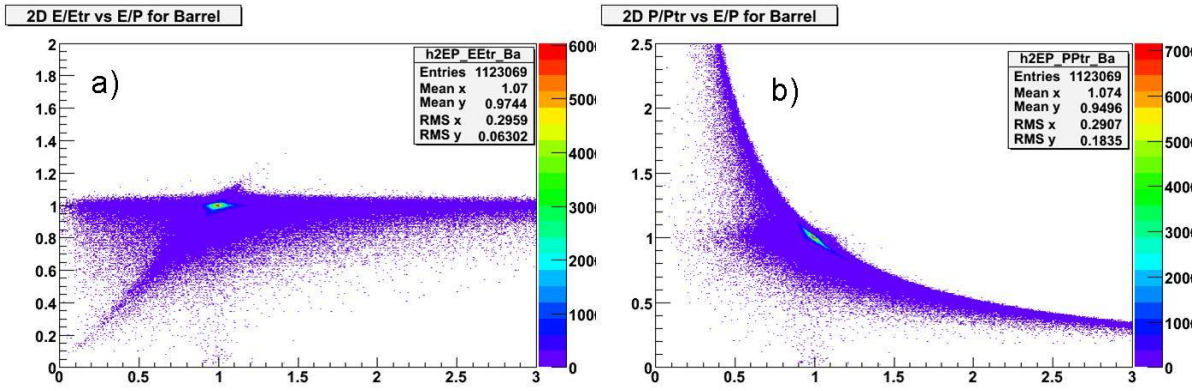

Figure 25: Estimation of the electron momentum from a) the ECAL and b) the Tracker as a function of E/p for electrons in the barrel.

We can distinguish in between three basis areas in the given plots. For

- $E/p < 1$ two components for the Tracker and the ECAL are found where the first and horizontal component represents a correct measurement of the electron momentum/energy whereas the second component represents a wrong estimation.

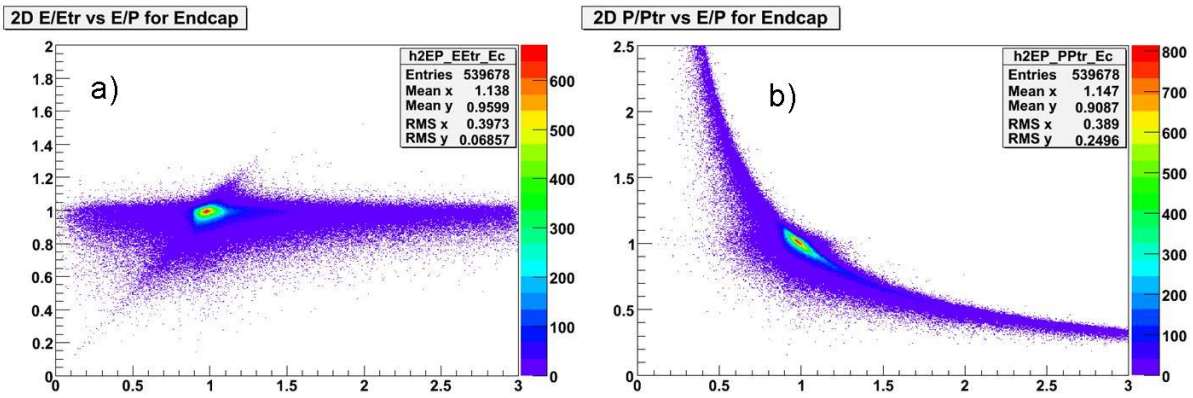

Figure 26: Estimation of the electron momentum from a) the ECAL and b) the Tracker as a function of E/p for electrons in the endcap.

- $E/p \approx 1$ the Tracker and the ECAL measure with a good accordance to the generated value
- $E/p > 1$ the ECAL estimation is mostly correct but the Tracker underestimates the electron momentum systematically.

With this consideration in mind the final electron momentum estimation is given as:

- When $|E/p - 1| < 2\sigma_{E/p}$: weighted mean of E and p

$$p_{final} = \frac{(E/\sigma_E^2) + (p/\sigma_p^2)}{(1/\sigma_E)^2 + (1/\sigma_p)^2} \tag{4}$$

  where σ_E is the error on the ECAL energy

- When $|E/p - 1| > 2\sigma_{E/p}$: E for $E > 15$ GeV and p for $E < 15$ GeV
- When $|E/p| < 1 - 2\sigma_{E/p}$: E for electrons of the Showering class and E for $E > 15$ GeV and p for $E < 15$ GeV for all other classes

With $\sigma_{E/p}$ calculated via error propagation:

$$\sigma_{E/p} = \sqrt{\left(\frac{\sigma_E}{p}\right)^2 + \left(\frac{E \cdot \sigma_p}{p^2}\right)^2} \tag{5}$$

For an examination of the effect of this combination, the effective RMS for $\frac{E-E_{true}}{E_{true}}$ is calculated in dependence of E. The effective RMS (σ_{eff}) is defined as the width of the distribution around the mean containing 68% of the number of events. Figure 27 shows the effective RMS for estimation of the ECAL and the Tracker and the result after combining these two estimations. The precision of the estimation has improved significantly in between 10 and 25 GeV. [3]

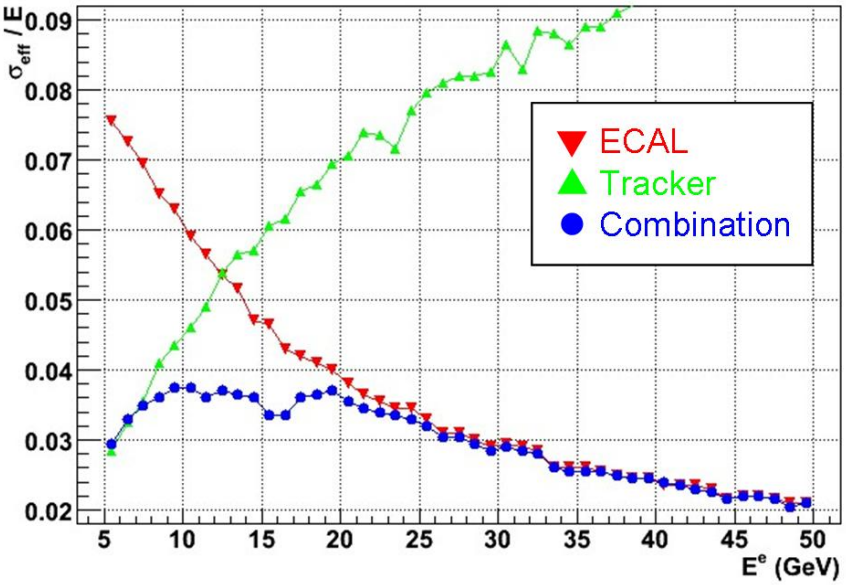

Figure 27: Effective RMS for the ECAL, the Tracker and the combined estimation for electrons in the barrel.

Despite from this clear improvement, two basic problems remain for the barrel:

1. At low energies the combined estimation is worse than the result of the Tracker alone

2. At 15 GeV we find an "unsteadiness hole" in the plot

The improvement for the endcap is not as high as for the barrel but still considerable. Below 20 GeV the distribution is quite unsteady and for 9 GeV even above the error for the Tracker (see figure 28).

In a two dimensional plot of the momentum after combination as a function of E/p it

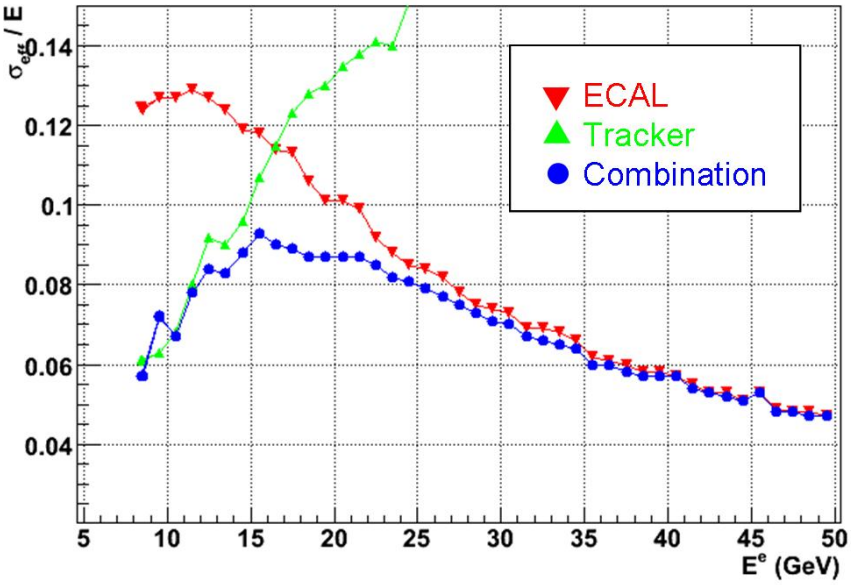

Figure 28: Effective RMS for the ECAL, the Tracker and the combined estimation for electrons in the endcap.

is found that for most events the combination gives a good estimation of the electron momentum. Still there are three main areas where the combination is not quite accurate which can be seen in figure 29 (more clearly for the barrel).

1. For values of E/p <1 sometimes the track momentum is taken although it overestimates the electron momentum,

2. For values of E/p <1 sometimes the ECAL energy is taken although it underestimates the electron momentum,

3. For values of E/p >1 sometimes the track momentum is taken although it underestimates the electron momentum

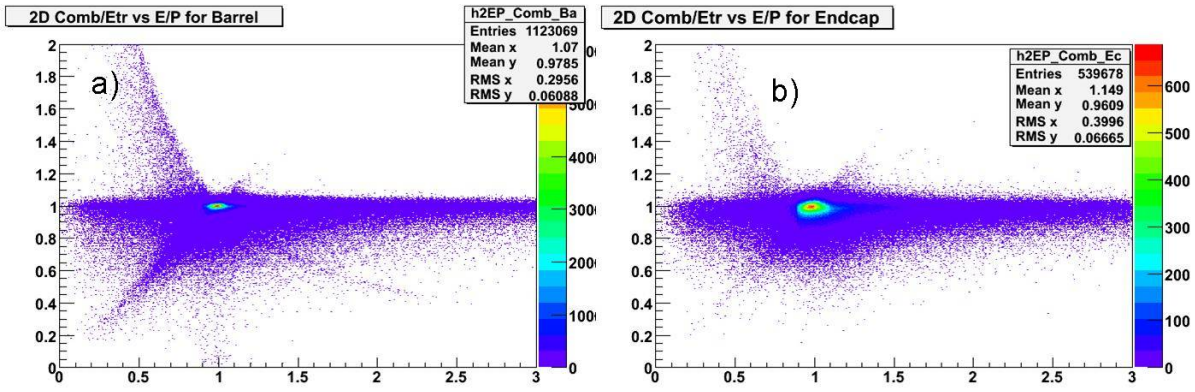

Figure 29: Combinated momentum estimation divided by E_{true} as a function of E/p for a) the barrel and b) the endcap.

4.2 New combination

4.2.1 Approach

As seen above, the combination introduced in 4.1 improves the estimations of the ECAL and the Tracker. By applying the corrections on the electron track momentum and the electron track momentum error (see section 3.3.2) the physics TDR combination is already improved since the estimations for the electron track momentum and its error are more accurate.
One of the main goals of the laboratory was to scan this combination for further improvements. To achieve that, a multilateral approach is chosen, consisting of:

1. a reconsideration of the above given threshold of the energy to decide between the estimations of the ECAL and the Tracker separated
   - by electron class
   - by endcap and barrel
2. an analysis of the chosen width of the combination area
3. a check for correlations as a function of η, E and ϕ

To look for dependencies E/E_{true} and p_{corr}/p_{true} are plotted versus the above mentioned parameters in two-dimensional plots.
1. In a first step an examination of E/E_{true} and p_{corr}/p_{true} as a function of E/p_{corr} with different thresholds for the electron energy shows that for $E/p_{corr} < 1 - 2\sigma_{E/p}$

the Tracker gives a considerable better estimation of the electron momentum than the ECAL for Showering electrons in the barrel up to energies of 18 GeV (see figure 30) as well as for Crack electrons up to 60 GeV (see figure 31). For the Golden electrons in the barrel the same conclusion can be drawn for values of $E/p_{corr} < 1 - 2\sigma_{E/p}$ or $1 + 2\sigma_{E/p} < E/p_{corr} < 1.15$ and energies below 15 GeV (see figure 32).

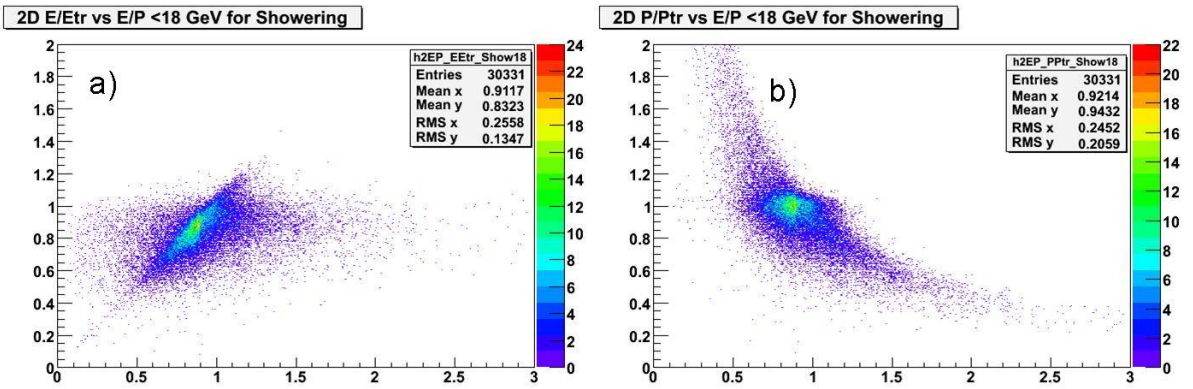

Figure 30: Distributions of a) E/E_{true} and b) p_{corr}/p_{true} as functions of E/p_{corr} for Showering electrons with an energy below 18 GeV.

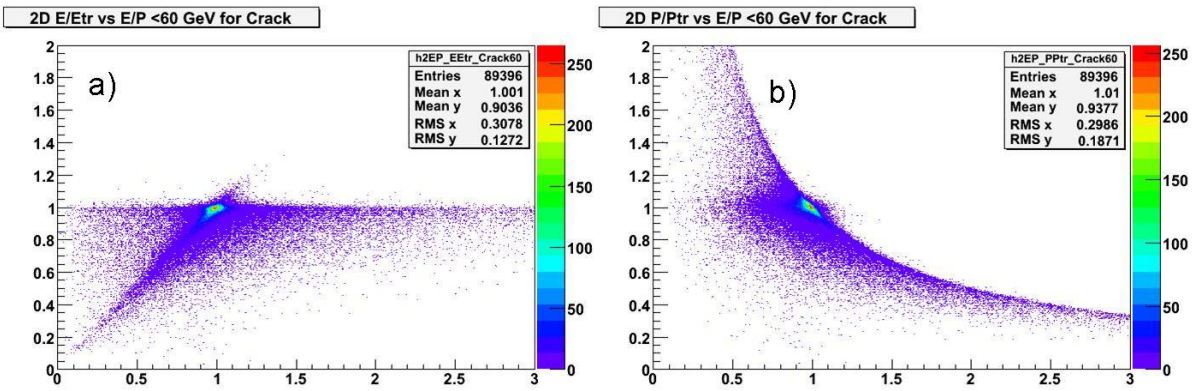

Figure 31: Distributions of a) E/E_{true} and b) p_{corr}/p_{true} as functions of E/p_{corr} for Crack electrons with an energy below 60 GeV.

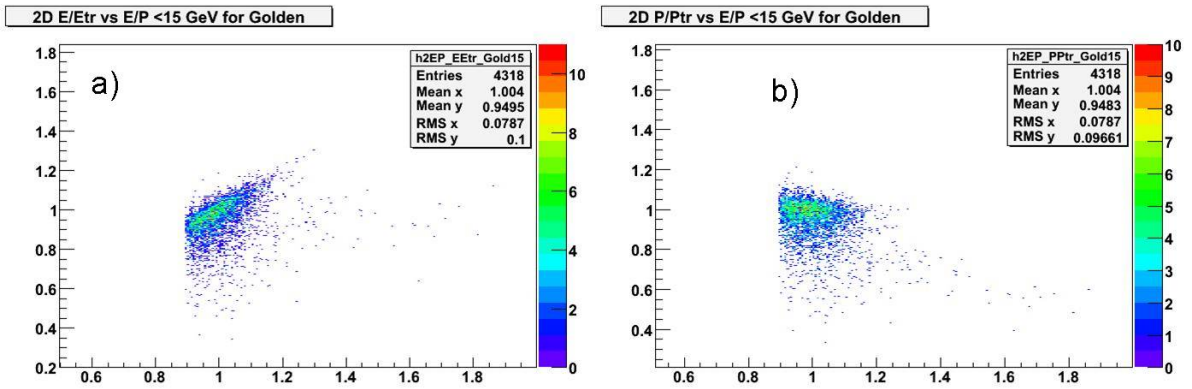

Figure 32: Distributions of a) E/E_{true} and b) p_{corr}/p_{true} as functions of E/p_{corr} for Golden electrons with an energy below 15 GeV.

2. In a second step the plots of the effective RMS are examined and redone for different values of the width of the combination area. The chosen value of $2.5\sigma_{E/p}$ is the one for which the effective RMS is the lowest, on average over the energy range.
3. At last the correlations between E/E_{tr} and η and ϕ are checked. Since there is already a classification for the η-crack electrons, no specific behaviour is found here around the boundaries in η. In contrary an effect for ϕ can be found. The energy is systematically underestimated for the electrons in the ϕ-regions between the modules as can be seen in figure 33. Like the crack-spaces between the modules in η the same exists for ϕ. Since the barrel is build of 18 Modules (in ϕ) the spaces in between appear each 20°. See also section 6.

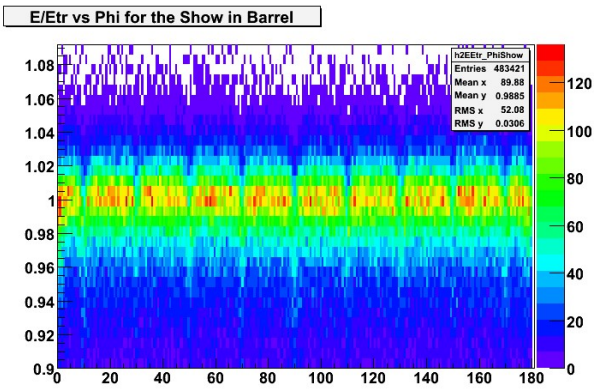

Figure 33: Distributions of E/E_{tr} as a function of ϕ for electrons in the barrel.

4.3 Applied changes

For the barrel the new electron momentum estimation is given as:

- When $|E/p_{corr} - 1| < 2.5 \cdot \sigma_{E/p}$: weighted mean of E and p after the corrections of p and σ_p

$$p_{final} = \frac{(E/\sigma_E^2) + (p/\sigma_p^2)}{(1/\sigma_E)^2 + (1/\sigma_p)^2} \tag{6}$$

- In all other cases E with the following exceptions:
  - For the Golden electrons: p for ($E < 15$ GeV and $E/p_{corr} < 1.15$)
  - For the Showering electrons: p for ($E < 18$ GeV and $E/p_{corr} < 1 - 2.5 \cdot \sigma_{E/p}$)
  - For the Crack electrons: p for ($E < 60$ GeV and $E/p_{corr} < 1 - 2.5 \cdot \sigma_{E/p}$)

For the endcap the new electron momentum estimation is given as:

- When $|E/p_{corr} - 1| < 2.5 \cdot \sigma_{E/p}$: weighted mean of E and p
- In all other cases E with the following exception:
  - For the Showering electrons: p for $E < 13$ GeV and $E/p_{corr} < 1 - 2.5 \cdot \sigma_{E/p}$

4.4 Results

As done above the effective RMS for $\frac{E-E_{tr}}{E_{tr}}$ is calculated in dependence of E. Figures 34 and 35 show the effective RMS for the estimation of the ECAL and the Tracker and the result after combining these two estimations after the correction of p and σ_p, with the new thresholds and width of the combination area.
For the barrel the precision of the estimation has improved for low energies and for energies in between 18 and 30 GeV. Moreover the unsteadiness hole has disappeared.
For the endcap the main improvement is a correction of the unsteadiness of the distribution.

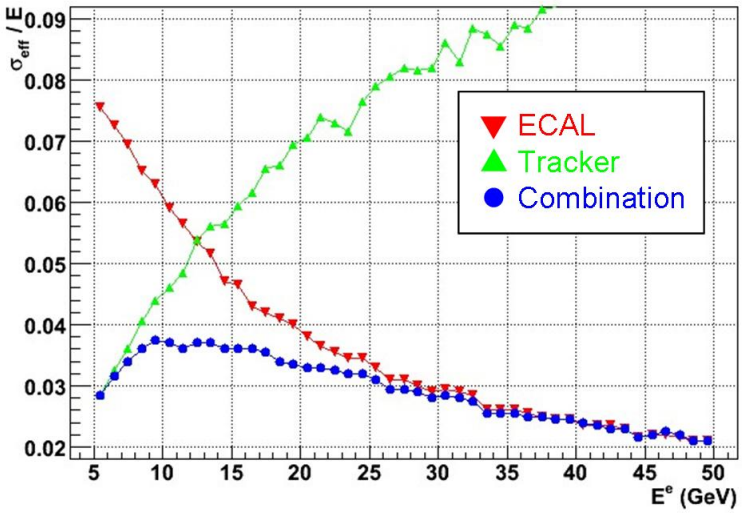

Figure 34: Effective RMS for the ECAL, the Tracker and the new combined estimation for electrons in the barrel.

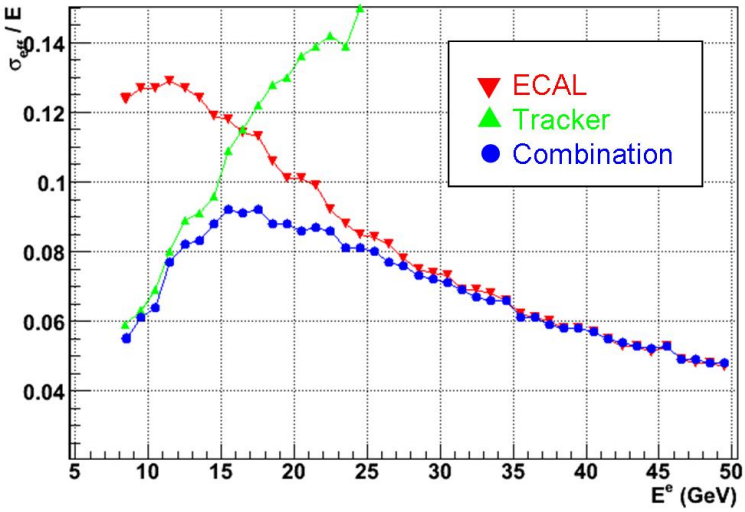

Figure 35: Effective RMS for the ECAL, the Tracker and the new combined estimation for electrons in the endcap.

As a comparison to section 4.1 the two dimensional plot of the momentum after combination as a function of E/p_{corr} is given (see figure 36). It can be seen that there are some more events in area 1, where the track momentum is taken although it overestimates the electron momentum, but area 2, where the ECAL energy is taken although it underestimates the electron momentum, and 3, where the track momentum is taken although it underestimates the electron momentum, almost disappeared.

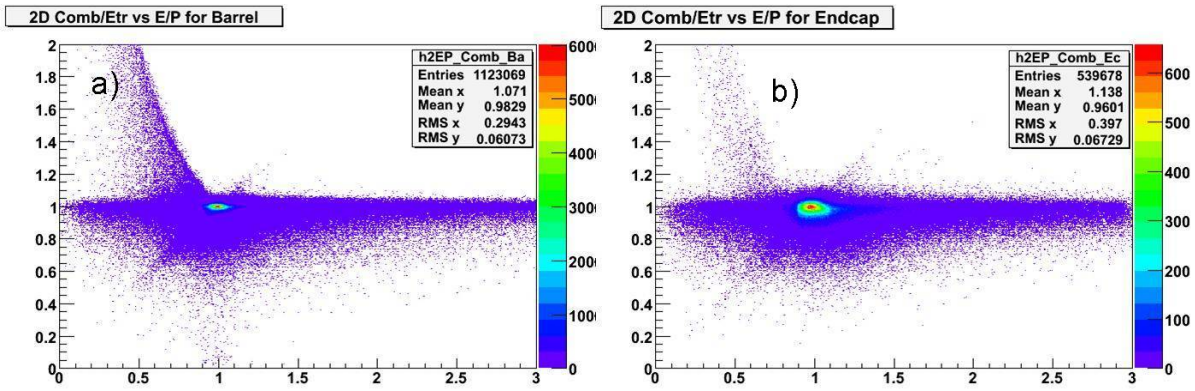

Figure 36: New combined momentum estimation divided by E_{true} as a function of E/p_{corr} for a) the barrel and b) the endcap.

5 Application

Since the principle goal was to improve the reconstruction of the Higgs boson invariant mass, a comparison of the reconstructed 4e invariant mass of the Higgs boson is made between before and after applying the results of this laboratory (see figure 37).

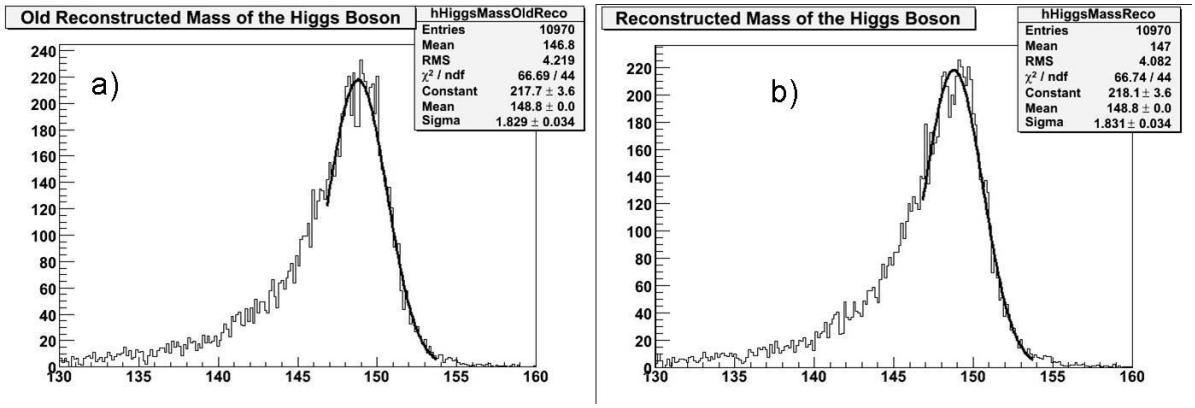

Figure 37: The reconstructed Higgs invariant mass with a) the old electron momentum estimation b) the new electron momentum estimation for a $H \rightarrow ZZ^* \rightarrow e^+e^-e^+e^-$ sample with $m_H = 150$ GeV.

The gaussian part of these two distributions is quite similar and can be concluded as almost the same by the values of the gaussian mean and sigma of the distributions. This is also proofed by the value of the effective RMS for the two plots, which is the same, equal to 4.30 GeV.
The values of the global mean and the RMS show a difference. The mean of the distribution of the reconstructed Higgs mass approaches the true value of 150 GeV by 0.2 GeV from $\bar{m_H} = 146.8$ GeV to $\bar{m_H} = 147$ GeV. Moreover the RMS was ameliorated by more than 3 % from a value of RMS=4.22 GeV to RMS=4.08 GeV. This leads to the conclusion that the new electron momentum is responsible for a reduction of the tail, for values that underestimated the Higgs mass of about 3% or more (as also can be seen in figure 38). This is also proved by the number of entries in the distribution of the reconstructed Higgs invariant mass between 130 GeV and 145 GeV. With the old electron momentum estimation, $n = 2306$ entries are found in contrast to $m = 2113$ entries with the new electron momentum estimation resetting from this laboratory, which is a reduction of more than 8%.

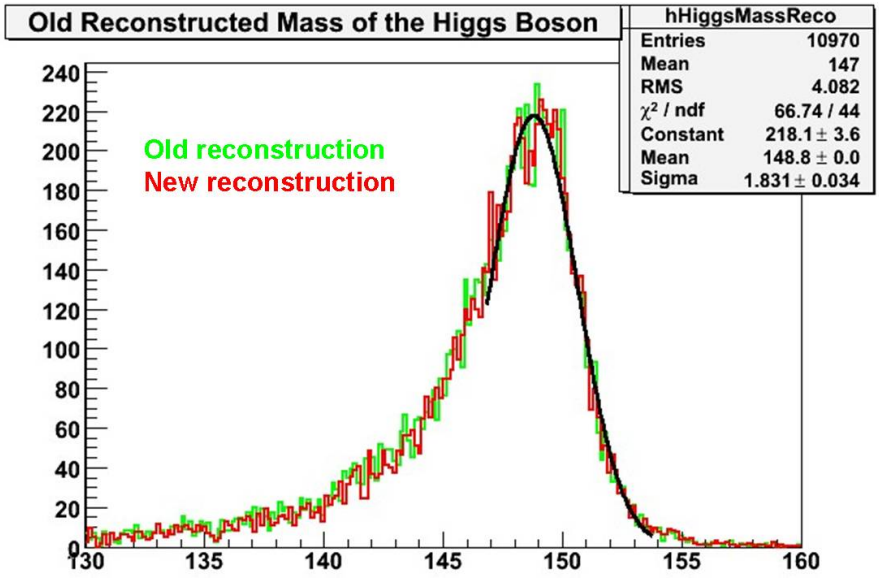

Figure 38: The reconstructed Higgs invariant mass with the old reconstruction and the new reconstruction.

6 Summary and outlook

After all the examinations given in this report one can conclude that the estimation of the electron momentum and its error as well as the combination of the energy of the ECAL and the track momentum could be slightly improved.
As an effect of the three components of this work (correction of p, σ_p and new E-p combination) the accuracy of the electron momentum measurement could be ameliorated up to 7% for low energies. This directly leads to a better reconstruction of the Higgs mass, where the percentage of underestimations are reduced by 8%, as is shown in section 5.
As mentioned in section 4.2.1 a correlation between E/E_{tr} and ϕ exists. Since it is planed in the CMS electron working group to take the ϕ-Crack electrons into account in the electron classification, it was decided not to apply a correction in the context of this laboratory. Nevertheless, the given E-p combination, and therefore the reconstruction of the Higgs boson invariant mass, could benefit directly from the new electron classification.
So after all the estimation of the electron momentum and its error as well as the combination of the energy of the ECAL and the track momentum is finally optimized with not much room left for further improvements.

References

[1] Wikipedia, "Large Hadron Collider", http://en.wikipedia.org/wiki/Large_Hadron_Collider, June 2007

[2] CMS collaboration, "CMS Physical Technical Design Report, Volume I", CERN/LHCC-2006-001

[3] S. Baffioni, C. Charlot, F. Ferri, D. Futyan, P. Meridiani, I. Puljak, C. Rovelli, R. Salerno and Y. Sirois, "Electron reconstruction in CMS", CERN-CMS-Note-2006-040, Eur.Phys.J.C.49:1099-116, 2007

[4] Peter W. Higgs, "Broken Symmetries and the Masses of Gauge Bosons", Phys. Rev. Lett., 13(16):508-509, 1964

[5] The LEP Electroweak Working Group, http://lepewwg.web.cern.ch/LEPEWWG/

[6] David J. Miller, "A quasi-political Explanation of the Higgs Boson for Mr Waldegrave, UK Science Minister", http://www.hep.ucl.ac.uk/∼djm/, 1993

[7] Gavin Hesketh, "Searches for the Standard Model Higgs at the Tevatron", Talk at Hadron Collider Physics Symposium, 2007

[8] S. Baffioni, C. Charlot, F. Ferri, N. Godinovic, P. Meridiani, I. Puljak, R. Salerno and Y. Sirois, "Discovery potential for the SM Higgs boson in the $H \to ZZ^{(*)} \to e^+e^-e^+e^-$ decay channel", CERN-CMS-Note-2006-115, J.Phys.634:N23-N46, 2007

[9] Claude Charlot, "La reconstruction des électrons dans CMS", thèse d'habilitation, 2007